Tellus
SERIES A
DYNAMIC
METEOROLOGY
AND OCEANOGRAPHY
PUBLISHED BY THE INTERNATIONAL METEOROLOGICAL INSTITUTE IN STOCKHOLM

Tellus (2009), 61A, 565–578
Printed in Singapore. All rights reserved

TELLUS

The 30–60-day oscillation in the East Asian summer monsoon and its time-dependent association with the ENSO

By KYUNG-SOOK YUN[1], BAOHUA REN[2], KYUNG-JA HA[1]*, JOHNNY C. L. CHAN[3] and JONG-GHAP JHUN[4], [1]*Division of Earth Environmental System, College of Natural Science, Pusan National University, Busan, Korea;* [2]*School of Earth and Space Sciences, University of Science and Technology of China, Hefei, China;* [3]*Guy Carpenter Asia-Pacific Climate Impact Centre, City University of Hong Kong, Hong Kong, China;* [4]*School of Earth and Environmental Sciences, Seoul National University, Korea*

(Manuscript received 16 December 2008; in final form 22 June 2009)

ABSTRACT

Based on 30–60-day oscillation in the East Asian summer monsoon (EASM), the relationship between its northward propagation and ENSO (El Niño and Southern Oscillation) was investigated. To explicitly describe the 30–60-day monsoonal evolution, an empirical orthogonal function (EOF) analysis was carried out on the temporal-latitude section of the longitudinal average for 115°E–120°E. The principal 30–60-day EASM mode captures a northward propagation of well-organized intraseasonal oscillation (NISO). Using the associated time series of the first mode, we found a significant lagged correlation between interannual variability of the NISO and ENSO. Its lagged correlations with NINO indices have a quasi-biennial (QB) characteristic through the preceding summer and the concurrent summer. Their relationship was found by the regression analysis relating the low-level circulation to the ocean temperature. The western North Pacific anticyclone and the anticyclone-induced easterly vertical wind shear anomalies induce the dynamical linkage between the NISO and QB-type ENSO. It is shown that the NISO is more closely tied with QB-type ENSO in its phase than in its amplitude, and may be connected to the anomalous easterly wind and the eastward evolution of an oceanic Kelvin wave, which is associated with abrupt ENSO transition. The predictability on ENSO and NISO is examined through the canonical correlation analysis.

1. Introduction

The East Asian summer monsoon (EASM), which is one of the extratropical monsoons, has not only interannual variability but also intraseasonal variation. It is also characterized by abrupt northward jumps and stationary periods (Wu and Wang, 2001). Climatologically, as the monsoon trough moves northward into East Asia, the EASM rainfall begins in early June over central China and Japan, in late June over Korea, and finally in early July over northern China (Ha et al., 2005). The interannual variations of large-scale circulations rely on the effect of the Tibetan Plateau (Nitta, 1983), tropical sea surface temperature (SST) (Zhang et al., 1996) and standing highs, such as the Bonin high and western North Pacific high (Ha and Lee, 2007). As the rainfall in the EASM tends to be concentrated in a limited region and a period during the summer, the information on intraseasonal oscillation (ISO) for the 30–60-day periodicity is important. Particularly, the northward propagating ISO plays a vital role in determining the timing of the active and break cycle of the monsoon system, according to the northward movement of the monsoon trough (e.g. Lau and Chan, 1986).

Typically, there are different ISO characteristics in different seasons. In the tropical region, the boreal summer ISO is weaker and more complex than the boreal winter ISO. During the boreal summer the ISO frequently propagates northward from the equator in the western Pacific (Wang and Rui, 1990). The ISO signal in the western North Pacific (WNP) propagates into East Asia. The northward propagating ISO in the boreal summer has been explained by the emanation of Rossby waves from enhanced deep convection (Hsu and Weng, 2001; Tsou et al., 2005). Many researchers including Kawamura et al. (1996) and Tsou et al. (2005) have emphasized the evolution and mechanism of the northward propagation of 30–60-day oscillation over East Asia. Particularly, Kawamura et al. (1996) have found that the strong convection activity over the Philippines contributes to the development of an extratropical ISO through a barotropic Rossby

*Corresponding author.
e-mail: kjha@pusan.ac.kr
DOI: 10.1111/j.1600-0870.2009.00410.x

wave emanation. It implies that the northward propagation of extratropical ISO over East Asia might be closely linked to the tropical circulation, such as El Niño and Southern Oscillation (ENSO).

A primary purpose of this study is to find the relationship between the northward propagation of the 30–60-day oscillation over East Asia and ENSO. Many studies have examined the relationship between ENSO and the interannual variability of the Madden-Julian oscillation (Madden and Julian, 1971) for the summer (Lawrence and Webster, 2001; Lu and Ren, 2005) as well as winter (Hendon et al., 1999; Slingo et al., 1999). However, the linkage between the northward propagating ISO in the EASM and ENSO has not been explicitly documented due to a difficulty in relating phenomena in different time and space scales. As a possible mechanism, Teng and Wang (2003) proposed a vertical wind shear mechanism where the vertical increase of ENSO-induced easterly wind anomalies in the western Pacific generates the northward emanation of Rossby wave, and in turn enhances the northward propagating ISO intensity. However, their study has been restricted to the relationship between May-October ENSO and tropical summer ISO. The long-term time lag relationship with ENSO has not been firmly examined. The possible lagged linkage between ENSO and interannual variability of the northward propagating ISO in the EASM is highlighted in the present study. In particular, to see the north-south evolution of the ISO, an empirical orthogonal function (EOF) analysis is carried out for a time-latitudinal section of 30–60-day filtered convection. This will provide the relationship of the ENSO to the phase and amplitude of the northward propagating ISO. Furthermore, the predictability between of the relationship between the ENSO and the northward propagating ISO is examined with canonical correlation analysis (CCA).

2. Data and methodology

2.1. Data and analysis

This study assesses the 30–60-day mode of outgoing long-wave radiation (OLR) data. The daily OLR data from 1979 to 2004 obtained from the National Oceanic and Atmospheric Administration were used for the EOF analysis to examine the northward propagation of monsoonal convection. We also used the National Center for Environmental Prediction/National Center for Atmospheric Research (NCEP/NCAR) reanalysis data (Kalnay et al., 1996) (from 1978 to 2004) and ocean temperature (Ji et al., 1995) (from 1980 to 2000) for the regressed relation with ENSO. The monthly Southern Oscillation Index (SOI) and NINO indexes from 1978 to 2004 were acquired from the National Oceanic and Atmospheric Administration/Climate Prediction Center. Monthly SST data were obtained through the British Atmospheric Data Centre/Hadley Centre Sea Ice and Sea Surface Temperature data set (Rayner et al., 2003).

The northward migration of the monsoonal front is modulated by the ISO, particularly the 30–60-day component (e.g.Chen and Chen, 1995; Tsou et al., 2005). Lau et al. (1988) have emphasized the importance of dynamics associated with the 30–60-day oscillation in the EASM. The significant 30–60-day periodicity is also detected by the spectral analysis (not shown). The analysis using the unfiltered data poses difficulties for selecting the northward propagating pattern of monsoonal evolution. In order to show more easily the interannual variability in the movement of the monsoonal front, the climatological seasonal cycle in daily OLRs was first removed and anomaly fields were filtered through a band-pass filter as described by Murakami (1979) to remove the high-frequency (<30 days) and low-frequency (>60 days) variations.

The ISO exhibits a strong amplitude in the longitudinal extent of 115°E-125°E. For the purpose to investigate the meridional evolution of ISO for the monsoonal convection, we focused on the sublongitudinal region over East Asia between 115°E and 120°E. It has been known that the interannual variability of the extratropical ISO exhibits a smaller amplitude compared to the tropical ISO (Hsu and Weng, 2001; Tsou et al., 2005). This is also shown in the time-latitude section averaged over the area of 115°E-120°E (Fig. 1a). Of particular interest is that the ISO variability shows the strongest gradient around 25°N. The ISO to the south of 25°N has considerably larger and more persistent amplitudes in comparison with that to the north of 25°N.

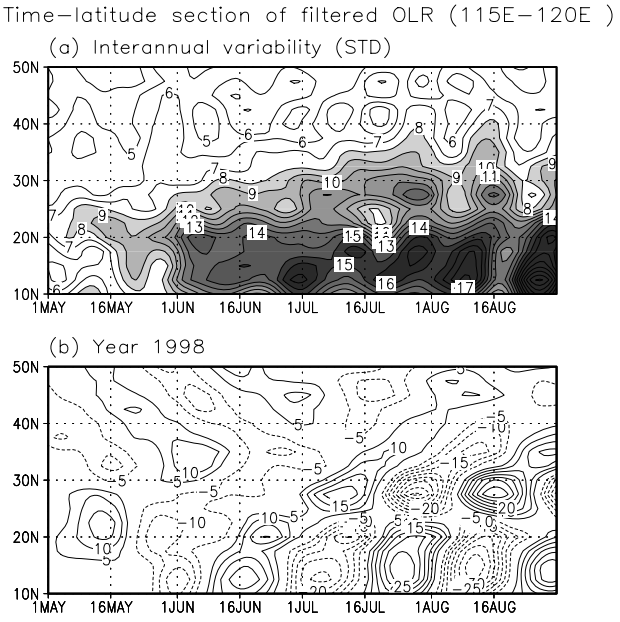

Fig. 1. The time-latitude section of (a) interannual variability (defined as year-to-year standard deviation) of the 30–60-day filtered OLR anomalies and (b) the 30–60-day filtered OLR anomalies in year 1998, which are averaged over the longitudinal area of 115°E-120°E. Shadings in (a) denote values greater than 8 W/m^2.

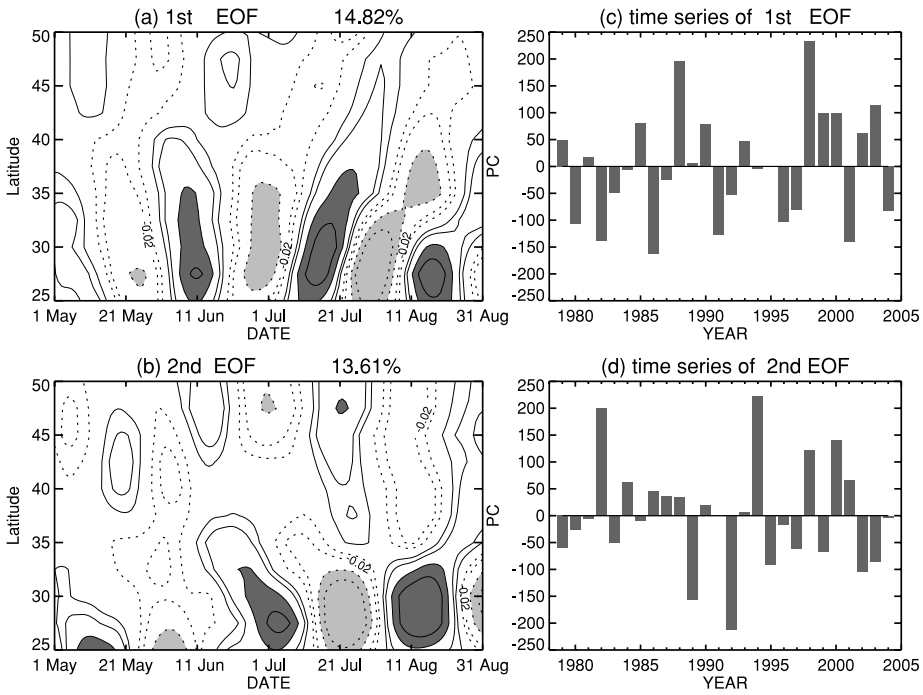

Fig. 2. (a) The first and (b) the second leading eigenvectors. The principal component time series of (c) the first and (d) the second eigenvectors obtained from the 30–60-day filtered OLR anomalies averaged in the longitude range of 115°E-120°E during 1979–2004. Heavy (light) shadings indicate values greater (less) than 1.5 (−1.5).

However, during specific years, the northern ISO signal has a meaningful variability. For example, during year 1998, there exists a substantial ISO variability north of 25°N, especially for late summer (Fig. 1b). The ISO anomalies north and south of 25°N are visibly out of phase. Some studies (e.g. Kawamura et al., 1996) support the existence of a significant extratropical ISO. For the investigation of the coherently propagating ISO in the EASM region, we chose the latitude domain of EOF as ranging from 25°N to 50°N. An EOF analysis was then carried out for a time-latitudinal section of a 30–60-day filtered OLR averaged over the longitudinal extent (3 points with 2.5° grid intervals) of the East Asia monsoon region (115°E-120°E). The EOF domain used in this study has a special structure composed of time and space. The reconstructed temporal-spatial EOF domain consists of the x-axis of the intraseasonal variance (from May to August) and the y-axis of the latitudinal variance (from 25°N to 50°N). The year-to-year variability for this domain represents the associated principal component (PC) time series. In general, the period of May to August involves different characteristics between early and late summers (e.g. Chang et al., 2000). We examined the entire summertime period (from May 1 to August 31) to observe the coherently propagating ISO component in summertime. The result for the EOF analysis in the space-time domain (Fig. 2) shows a considerable and reasonable evolution.

In order to investigate the relationship between the northward propagating ISO and ENSO, we applied a regression method in which the correlation coefficient was multiplied by the standard deviation of variable. Regressed features of the circulation and ocean temperature against their associated time series indicate a relationship between interannual variability of the ISO and ENSO. The Student's *t*-test was also applied to evaluate the significance of the regressed field with 24 degrees of freedom (i.e. 26 years).

2.2. *The CCA method*

In this study, a canonical correlation analysis (CCA) is performed in order to discuss the predictability between the northward propagation of the ISO and ENSO. The CCA technique is a multivariate statistical model that computes linear combinations of a set of predictors that maximizes their relationships to similarly calculated linear combinations of a set of predictands (Yu et al., 1997). The CCA and the EOF analysis have similar objectives and mathematics each other. Particularly, the CCA contains a set of eigenvectors (the loading patterns) for the predictor and predictand and a set of time series for each, whose temporal correlation is related to the amount of cross dataset variance explained by the mode (He and Barnston, 1996).

Consider the predictor matrix (X) and predictand matrix (Y) given by a function of space and time (from Yu et al., 1997). Performing EOF analysis on the predictor and predictand, X and Y are expressed by eigenvectors of EOF (E_X, E_Y) and their associated PC time series (t_X, t_Y).

Here, we can take the first k-th EOF modes so that the covariance matrix (A) of correlation coefficients between two PC time series has the largest value, and then obtain the canonical component time series as an input to the CCA model. Towards this goal, we use the singular value decomposition (SVD) method, which maximizes the covariance between the PCs. Then, as the linear combination between the canonical component time series ($T_{X,i}$, $T_{Y,i}$) and the canonical vector ($U_{X,i}$, $U_{Y,i}$) where $T_{X,i}$ $U_{X,i}$ $A_i = T_{Y,i}$ $U_{Y,i}$, $i = 1, k$, the predictand time series ($\widehat{T}_Y$) can be calculated as follows:

$$\widehat{T}_Y = (U_Y)^{-1} A U_X T_X \tag{1}$$

Using the orthogonal characteristics of EOF modes, the predictand values ($\widehat{Y}$) can be transformed as below:

$$\widehat{Y} = E_Y (U_Y)^{-1} A U_X (E_X)' X \tag{2}$$

Details are described by Yu et al. (1997) and He and Barnston (1996).

3. Northward propagation of the ISO over East Asia

The 30–60-day ISO during the boreal summer can be characterized by the northward propagation of the EASM. Generally, the coherent ISO activity was based on the most dominant EOFs (Hendon et al., 1999). We carried out an EOF analysis to investigate the principal structure of the northward propagating ISO and its interannual variability. The first two EOFs (Fig. 2) explain about 28.0% of the total variance. The EOFs show the seasonal structure of the ISO active/break cycle. The sign and absolute values of the PCs indicate the phase in the ISO and their amplitude in the phase, respectively, as interannual variability of the ISO. In this study, we investigate the change in both phase and amplitude.

In the temporal-spatial structure of the first EOF mode, positive and negative values occur alternatively with time from 25°N to 35°N, and this phenomenon has a relatively short period, of about 35 days. The positive-negative oscillation appears after late May. The ISO before late June exhibits a standing or southward propagating pattern. After July, the ISO appears to propagate northward. The characteristics of the boreal summer ISO in the WNP is dominant by eastward propagating components during May-July and northward propagating components during July-October (Teng and Wang, 2003). The first EOF in 1998 appears as the strongest amplitude (Fig. 2c). A negative value in the preceding year (1997) abruptly changes to a positive value in 1998 (1997/1998 El Niño is the most well-known ENSO event.).

While in the first EOF the oscillating characteristics appear as a regular structure extending to higher latitude, in the second EOF the ISO signal exhibits an irregular propagating structure and it stays mainly in the south of 32.5°N. This means that the first mode reasonably captures the northward propagating ISO variability in the EASM region in comparison with the second mode. Additionally the second mode does not show any significant relationship with ENSO (not shown). Therefore, we focus on the first leading EOF (that is, 30–60-day EASM mode) in order to establish the characteristics of the onset and retreat as well as the periodicity. The first leading EOF is defined as the northward propagation of the ISO (hereafter, referred to as NISO). The active/break phases in the first EOF resemble the climatological ISO cycle (not shown). It is noted that the extremely wet and dry phases of climatological ISO indicate climatological active/break monsoons. The active/break ISOs embedded in the seasonal cycle stem from a significant northward progressing climatological ISO for the active/break monsoons, which is in turn responsible for the seasonal structure of the summer monsoons (Wang and Xie, 1997).

4. Relationship between NISO and ENSO

In this section, we investigate the relationship between the interannual variability of the NISO and ENSO by calculating the lag correlations for monthly SOI and NINO indexes (Fig. 3). The reference period of the NISO is denoted by the thick grey bar in Fig. 3. For example, the negative time lag denotes that SOI and NINO indexes lead NISO. It should be noted that interannual variability of the NISO has a lagged relationship with ENSO. During the previous summer, a positive correlation between interannual variability of the NISO and ENSO SST (NINO1 + 2 and NINO3) is found, which is significant at the 95% confidence level. The negative correlation appears after the concurrent

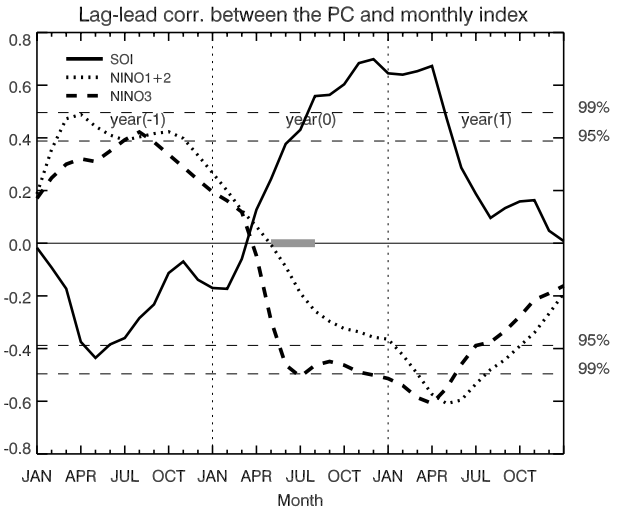

Fig. 3. Lag-lead correlation coefficients between the PC1 obtained from the 30–60-day OLR anomalies and one of the following index; monthly SOI, monthly SST anomaly in NINO 1 + 2 region and that in NINO 3 region. The reference NISO is displayed by a thick grey bar and year (−1) (year (1)) denotes the year before (after) the reference NISO.

summer, and reaches its apex in the following winter and spring. Barnett (1991) noted that the variability of ENSO can be explained in terms of the two dominant time scales. One is the quasi-biennial (QB)-type ENSO with a typical period of 2–3 years and the other is low-frequency (LF)-type ENSO of 4–5 years period. The QB-type ENSO is closely linked to the reversals of El Niño and La Niña events and thus imposes a regularity onto the ENSO physical cycle (Rasmusson et al., 1990). While the LF-type ENSO does not change with season conspicuously, the QB-type ENSO varies seasonally (e.g. Wang and An, 2005). The LF-type ENSO seems to account for the recent warming events and the interdecadal change in the tropical region (Kim, 2002; Wang and An, 2005). Additionally, the QB-type ENSO leads to the much stronger dynamical ocean response (i.e. Kelvin and Rossby waves) than the LF-type ENSO (Kim and Kim, 2002). This dynamical response plays a vital role in initiation and termination of the ENSO condition. It is noteworthy that the singularity for each ENSO event is mainly caused by the different relative importance of the two dominant modes (Kim, 2002). The interannual variability of the NISO is closely related to the QB-type ENSO, in remarkable agreement with the work of Shen and Lau (1995). They showed the strong biennial correlation between EASM rainfall and ENSO: a strong EASM is preceded by El Niño in the previous year. This signal is changed from the monsoon summer to the following winter/spring, leading to La Niña. Although the periodicity does not exactly correspond to the QB cycle, the correlation is shown by the La Niña developing years followed by El Niño developing years with a QB-like periodicity (2–3 years). In order to emphasize the transition of ENSO phase, we referred to 'ENSO' as 'QB-type ENSO'. The relationship resembles a tropospheric biennial oscillation (TBO), as shown in Yasunari (1990) and Meehl (1997), which relates to a large-scale east-west circulation from tropical Indian to tropical Pacific region with a periodicity of 2–3 years.

With regards to the QB-type ENSO, the seasonal evolution in SST and circulation field may suggest the dynamics associated with a development and decaying of El Niño/La Niña (Barnett, 1991). To illustrate the time-dependent seasonal evolution with QB-type ENSO, we have regressed the seasonal sequence from the preceding spring to the following winter for the unfiltered SST, geopotential height at 850 hPa and ocean temperature anomalies onto the first PC time series. Note that the PC time series exhibit the annual behaviour of the active/break cycle as the seasonal average statistic (shown by the NISO). Overall, the findings show that SST anomalies display positive (negative) values in equatorial eastern (western) Pacific regions from MAM(−1) to DJF(−1) (Fig. 4). The positive (negative) anomalies in the Philippine Sea (equatorial western Pacific) gradually propagate to the east. After the current summer (JJA(0)), the anomaly pattern is opposite to the one in the previous summer, and the negative anomalies strengthen until the winter (DJF(0)).

Figure 5 shows the regressed relation between geopotential height and wind anomalies at 850 hPa. There are high-pressure anomalies in the tropical western Pacific (in the longitudinal range of 110°E and 160°E) during the preceding summer. In the same manner as geopotential height anomalies, there are westerly wind anomalies (i.e. weakened easterly) in the equatorial central Pacific. Although the high-pressure anomalies are not significant in all seasons, the significant high-pressure anomalies move from the tropical western to eastern Pacific between the preceding summer (JJA(−1)) and the concurrent summer (JJA(0)). After the concurrent summer, low-pressure anomalies in the tropical western Pacific (i.e. 110°E-160°E) appear to be developing and propagating eastward until DJF(0). The apparent east-west circulation pattern in the equatorial region exists in DJF(0). The easterly wind anomalies (i.e. enhanced easterly) in the equatorial western/central Pacific are evident after the concurrent summer (JJA(0)). These easterly wind anomalies occupy an expanded area until DJF(0). The most important factor is the significant anticyclonic flow in the WNP (i.e. 120°E-160°E, 10°N-30°N) during the concurrent summer. The enhanced WNP high occurs with the westward extension. The anticyclonic anomalies are likely to play an important role in connection with QB-type ENSO. The vital role of the summertime anticyclonic anomalies mentioned above will be suggested in Fig. 8. According to the anomalous anticyclone in the WNP, anomalous easterly winds occur in the western Pacific. The equatorial wind anomalies in the western Pacific are known to play an important role in the decay of eastern Pacific SST anomalies related to the ENSO turnover (i.e. El Niño to La Niña) (e.g. Kug and Kang, 2006). The anomalous easterly winds in the western Pacific induce the upwelling in connection with an oceanic Kelvin wave, which is followed by abrupt transition of the ENSO phase. This association with an oceanic Kelvin wave is shown in Fig. 6.

The QB-type ENSO indicates that El Niño phase (or La Niña phase) abruptly takes a transition into the opposite phase in the period of QB. The important part of the abrupt transition is an anomalous heat source in the ocean (e.g. Meehl, 1997). Particularly, the eastward evolution and transition of ENSO phase are related to the oceanic Kelvin wave associated with anomalous wind forcing in the western Pacific. We obtained the regressed ocean temperature fields against the interannual variability of the NISO along the equatorial (5°N-5°S) band (Fig. 6). During the preceding year, there were negative anomalies in the western Pacific and positive anomalies in the eastern Pacific. The significant negative anomalies moved slowly eastward from JJA(−1) to MAM(0). The eastward propagation of anomalies is normally associated with an oceanic Kelvin wave. In the present study, the upwelling due to the oceanic Kelvin wave seems to be manifested as negative temperature anomalies across the eastern Pacific. Then, the negative anomalies strengthen and evolve after the concurrent summer (JJA(0)). As a result, the largest negative anomalies occur in the winter and the following spring. These

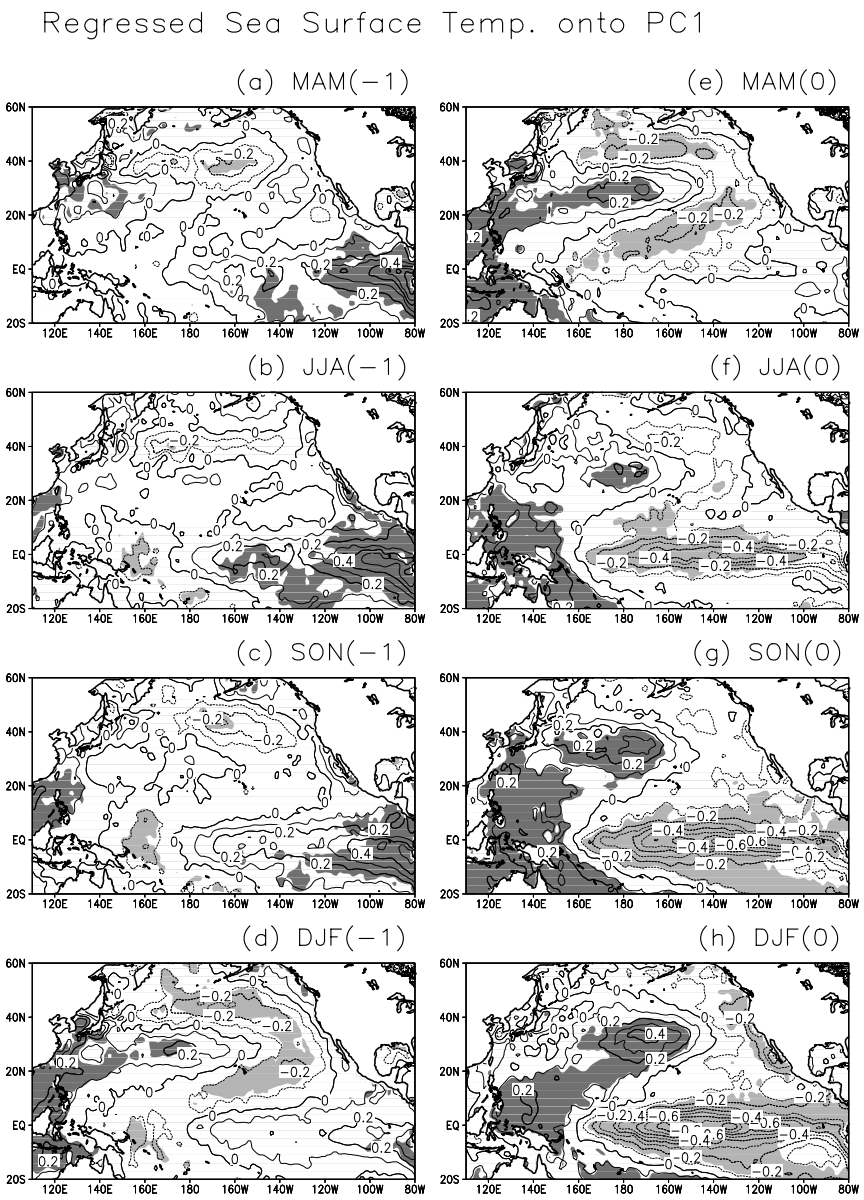

Fig. 4. The seasonal sequence for regressed fields of the sea surface temperature against PC1 obtained from the 30–60-day OLR anomalies. Heavy (light) shadings denote positive (negative) SST anomalies significant at a 95% confidence level.

patterns during the concurrent year have very similar features one another but opposite signs from those during the preceding year, implying an ENSO phase transition.

Consequently, the relationship between NISO and ENSO occurs with the abrupt change in the ENSO phase through the anomalous easterly wind and the upwelling associated with oceanic Kelvin waves. In order to support the association of the NISO with the ENSO transition, we have performed a composite analysis of the 30–60-day ISO for positive ENSO transition cases (i.e. El Niño to La Niña/neutral) and negative ENSO transition cases (i.e. La Niña/neutral to El Niño) (Fig. 7). Here, the El Niño (La Niña) year is defined in terms of an NINO3 index more than 0.5 (less than −0.5). The remaining years belong to be neutral years. The ENSO phase is separately classified as the non-El Niño (La Niña or neutral) year or the El Niño year. Extreme years are as follows: the positive transition cases are 1983, 1988, 1992, 1995, 1998 and 2003; the negative cases are 1982, 1986, 1991, 1994, 1997 and 2002. For example, the case 1982 corresponds to non-El Niño 1981/82 winter and El Niño 1982/83 winter. We applied the Student's *t*-test with 10 degrees of freedom (i.e. 6 positive and 6 negative transition years) to show the statistical significance of the composite difference for positive versus negative ENSO transition years. In the strong ENSO transition years, the ISO exhibits larger difference in the

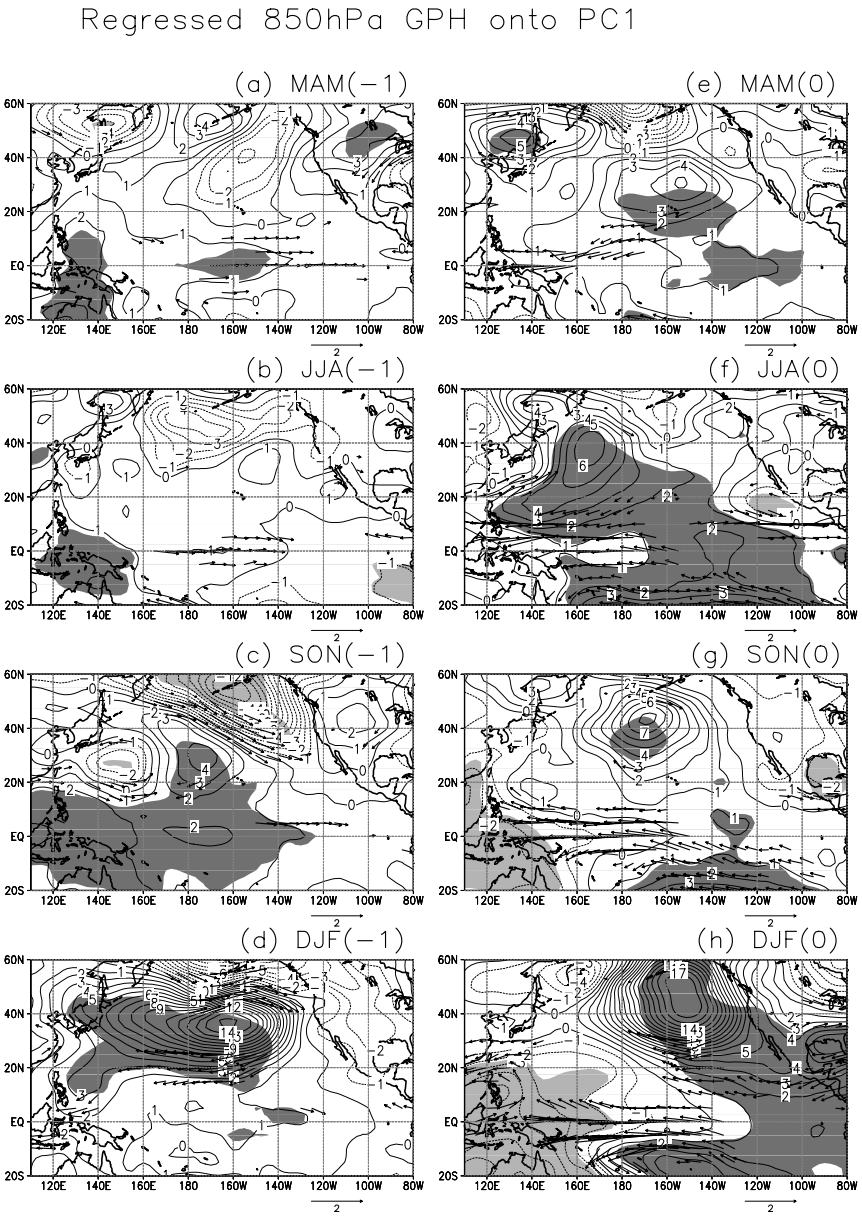

Fig. 5. Same as Fig. 4 except for geopotential height at 850 hPa. Heavy (light) shading denotes positive (negative) height anomalies significant at a 95% confidence level. The arrows indicate the 850-hPa wind anomalies significant at a 90% confidence level.

phase than in the amplitude. Although ISOs for ENSO transition years (including both positive and negative transitions) show reasonably large amplitude as compared with those for the normal years (i.e. the remaining years), the difference in the amplitude is somewhat smaller than that in the phase (not shown). The phase is quite similar to the one in the first EOF, though the signal appears in the south of 40°N (Fig. 2a). In comparison with the climatological ISO (i.e. a 30–60-day filtered OLR anomaly from climatological daily mean), the composite fields for positive versus negative ENSO transition years exhibit the notable difference in phases. For example, in reference to the negative anomalies around mid-June for climatological ISO, the negative anomalies for positive (negative) years appear in a delayed (earlier) phase around late June (early June). It indicates a significant dependency of NISO on the ENSO transition.

In summer followed by the preceding El Niño, the significant anticyclonic anomalies appear in the WNP (see Fig. 5). Regarding the QB-type ENSO, the development of the WNP high can be modulated by the large-scale Hadley and Walker circulations and the local air–sea interaction (Shen and Lau, 1995; Chang et al., 2000). In particular, Wang and An (2005) found that the spatial pattern of QB-type ENSO corresponds

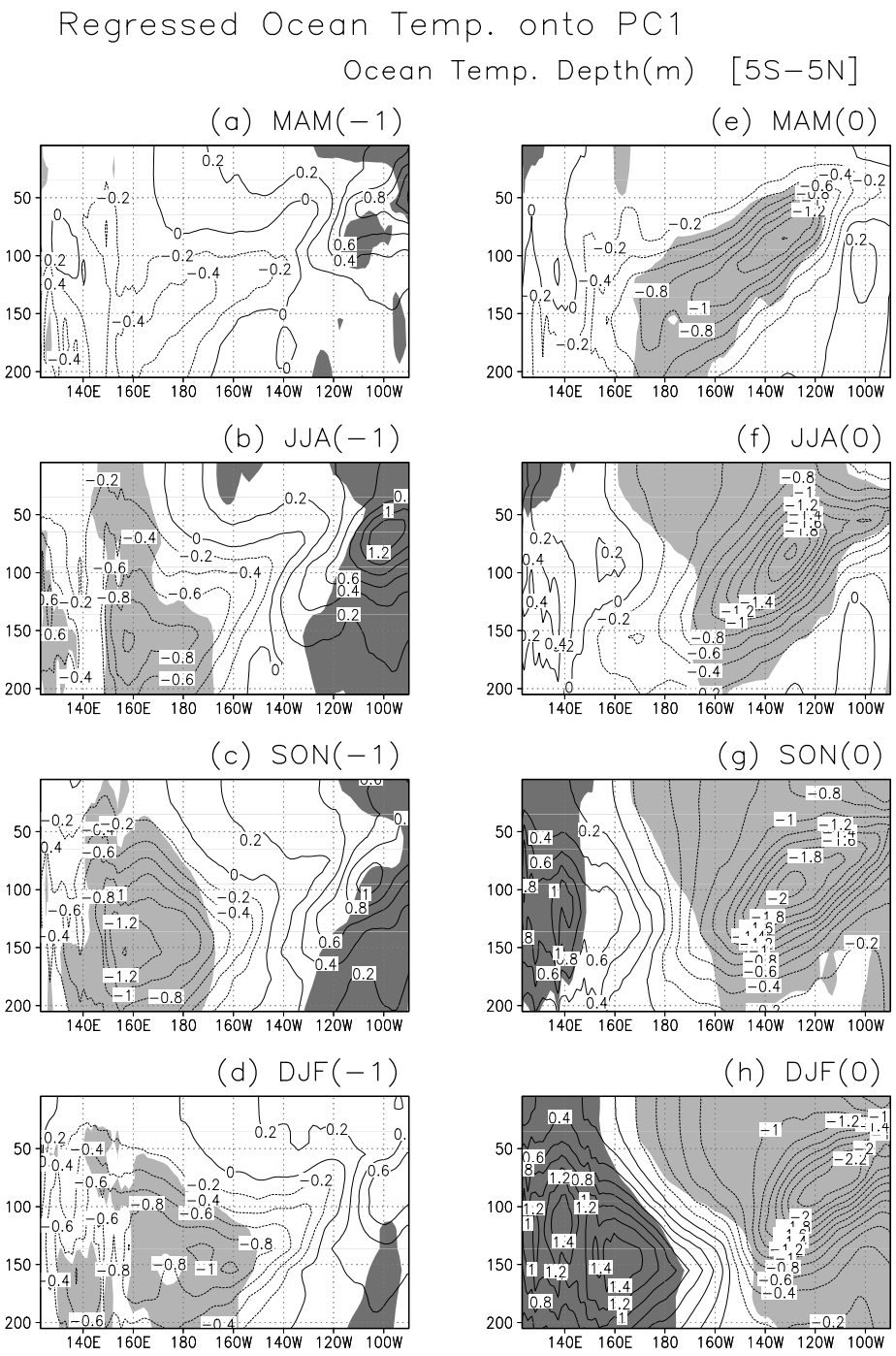

Fig. 6. The seasonal sequence for regressed vertical fields of the ocean temperature anomalies along the equatorial belt (5S-5N) against the PC1 obtained from the 30–60-day OLR anomalies. Heavy (light) shading denotes positive (negative) anomalies significant at a 95% confidence level.

to the dominant mode of Asian-Australian monsoon (shown in Wang et al., 2003), which is characterized by the anomalous WNP anticyclone. Li et al. (2007) showed that WNP anticyclonic anomalies are more closely linked to ENSO events with the abrupt phase transition than those without abrupt transition. The easterly anomaly along the southern edge of the WNP high contributes to the termination of El Niño. Consequently, the anomalous WNP high may play an important role in explaining the dynamics on the reversals of El Niño/La Niña and in turn QB-type ENSO. We regard the WNP high as a vital intermediator that connects the NISO and QB-type ENSO. To explain this, we have performed the composite analysis of the 850 hPa

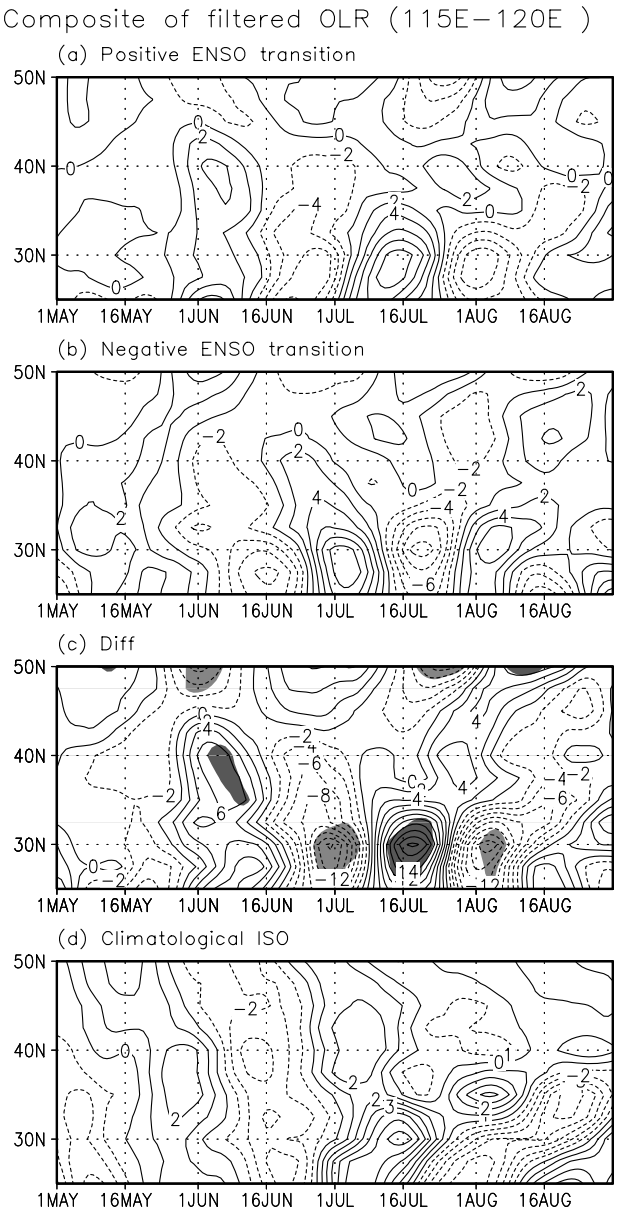

Fig. 7. The time-latitude section of the 30–60-day filtered OLR anomalies averaged in the longitude range of 115°E-120°E for (a) positive ENSO transition, (b) negative ENSO transition and (c) the difference (positive minus negative). (d) The climatological ISO anomalies averaged in the longitude range of 115°E-120°E. Heavy (light) shadings denote positive (negative) anomalies significant at a 95% confidence level.

geopotential height and vertical wind shear (i.e. U200-U850) anomalies averaged over the broad longitude range of 115°E-140°E for the positive and negative ENSO transitions (Fig. 8). There are significant height differences centred at approximately 20°N (Fig. 8c). Along the southern (northern) edge of anticyclonic flow, the low-level anomalous easterly (westerly) wind appears in Fig. 8f and consequently the easterly wind shear is weakened (strengthened).

Wang and Xie (1996) proposed a vertical shear mechanism associated with the baroclinic and barotropic components of equatorial wave motion (i.e. Rossby and Kelvin wave). The vertical shear of zonal flow acts to force the emanation of heating-induced barotropic Rossby waves towards the north. Jiang and Waliser (2008) represented the primary process of easterly shear using a simple equation of the vorticity as follows:

$$\frac{\partial \zeta_+}{\partial t} = -\beta v_+ - \bar{U}_T \left(\frac{\partial w}{\partial y} \right) \tag{3}$$

Here, β represents the meridional gradient of Coriolis parameter, '+' denotes the barotropic components of the meridional wind (v) and vorticity (ζ). With easterly wind shear ($\bar{U}_T < 0$), positive barotropic vorticity tendency appears to the north of the heating because of the northward decrease of upward vertical motion ($\partial w/\partial y > 0$). The positive barotropic vorticity then induces a low-level moisture convergence due to Ekman pumping, which creates the emanation of barotropic Rossby wave towards the north. Furthermore, Lu and Ren (2005) have shown that the weakened easterly shear in the tropical region delays the phase of the ISO. In the same manner, the strengthened easterly shear may advance the NISO in the EASM, inducing the difference in phases. Of particular interest is the onset timing in the height and vertical shear anomalies. After late June, significant easterly shear anomalies appear and are roughly consistent with the time of the northward propagation of ISO signals (see Fig. 2).

5. Predictability of ENSO and NISO

The abrupt transition of ENSO has a significant effect on the temporal-spatial pattern of the NISO. The leading mode of the NISO in the EASM is closely associated with eastern Pacific SST anomalies in the preceding summer and the ensuing winter or spring. The canonical correlation analysis (CCA, Section 2.2) is performed based on results described above in order to discuss the predictability between the NISO and ENSO. The diagnostic approach using the CCA technique has been proved to be an effective method for temperature or precipitation forecasts in the tropics (He and Barnston, 1996) and the mid-latitudes (Hwang et al., 2001).

Here, we used 10 modes of EOFs, which explain about 82% of total variance for NISO and about 97% for SST. The eastern Pacific SST anomalies in the preceding summer are used as a predictor of the NISO. The first leading EOF patterns and the associated PC time series for the concurrent summer NISO and the preceding summer SST anomalies are shown in Fig. 9. The predictor's domain is chosen as 160°E-100°W, 15°S-15°N, including the central/eastern Pacific. The predictand's domain is the same as in the previous analysis (Fig. 2). Here, we used the SST (30–60-day filtered OLR) dataset from 1978 to 2002 (from 1979 to 2003). Strong positive SST anomalies in the central/eastern

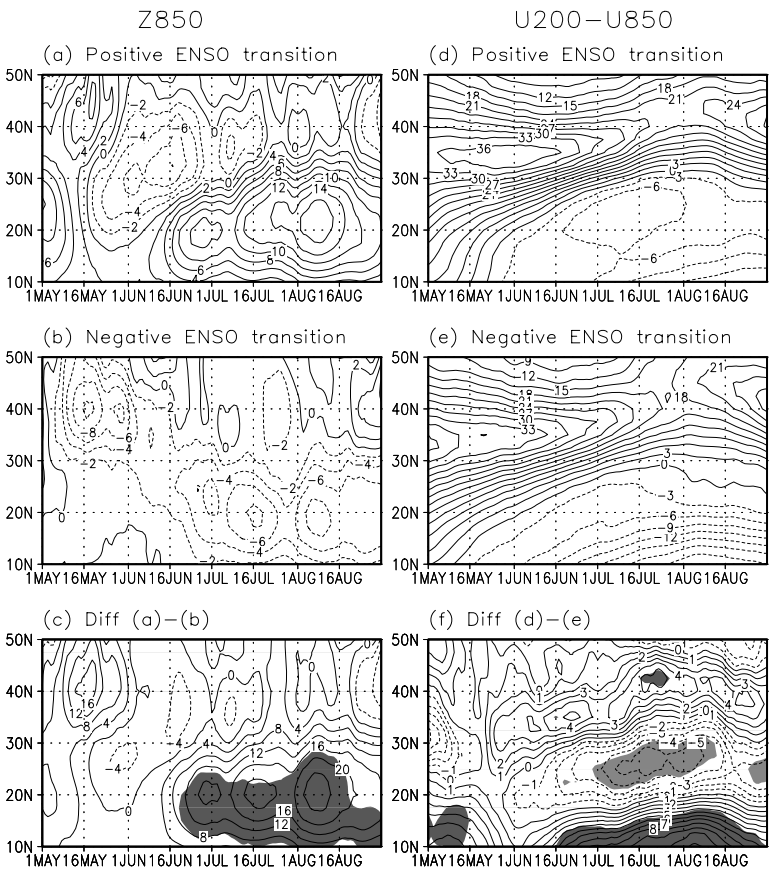

Fig. 8. The time-latitude section of (a)–(c) the 850-hPa geopotential height and (d)–(f) vertical wind shear (U200-U850) anomalies averaged in the longitude range of 115°E-140°E for positive ENSO transition ((a) and (d)), negative ENSO transition ((b) and (e)) and the difference ((c) and (f)). Heavy (light) shadings in (c) and (f) denote positive (negative) anomalies significant at a 95% confidence level.

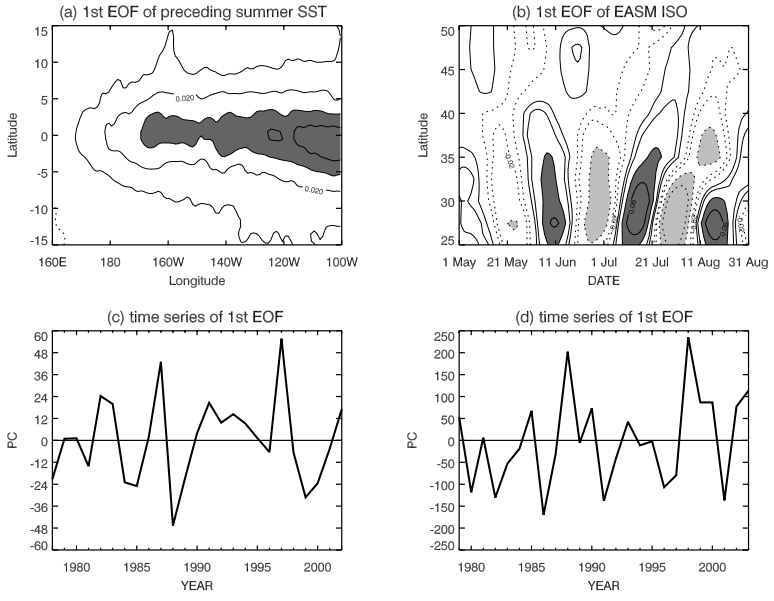

Fig. 9. The first leading eigenvector of (a) SST anomalies in the preceding summer (predictor) and (b) NISO (predictand), and the associated time series for (c) SST and (d) NISO.

Pacific are associated with the meridional structure of the ISO. The associated time series of the NISO is correlated to the Pacific SST time series for the first EOF mode with a positive correlation (about 0.39). That is, warmer SST anomalies in the preceding summer are related to positive NISO phase (shown in Fig. 2a). The two canonical component time series have a correlation coefficient of about 0.60 (Fig. 10). The greater the correlation between the canonical component time series of the predictor and

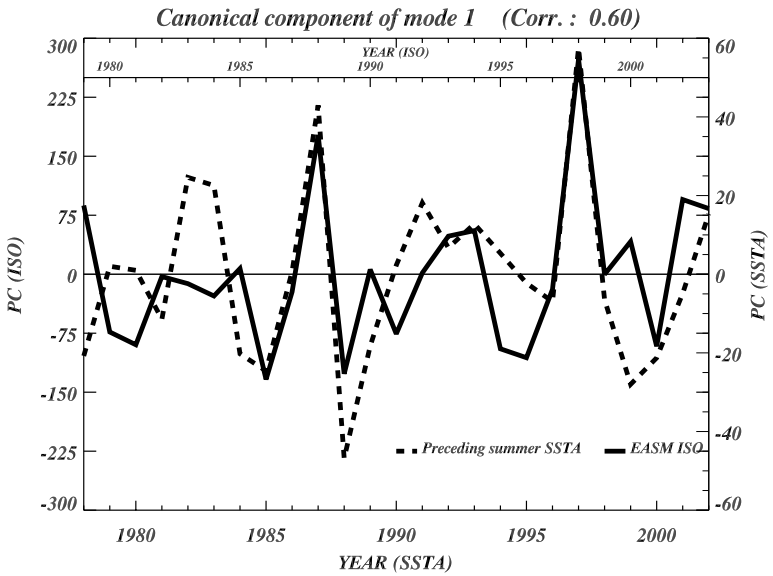

Fig. 10. The canonical component time series of mode 1. The solid and dashed lines indicate the values for the NISO in the EASM and the preceding summer SSTA, respectively.

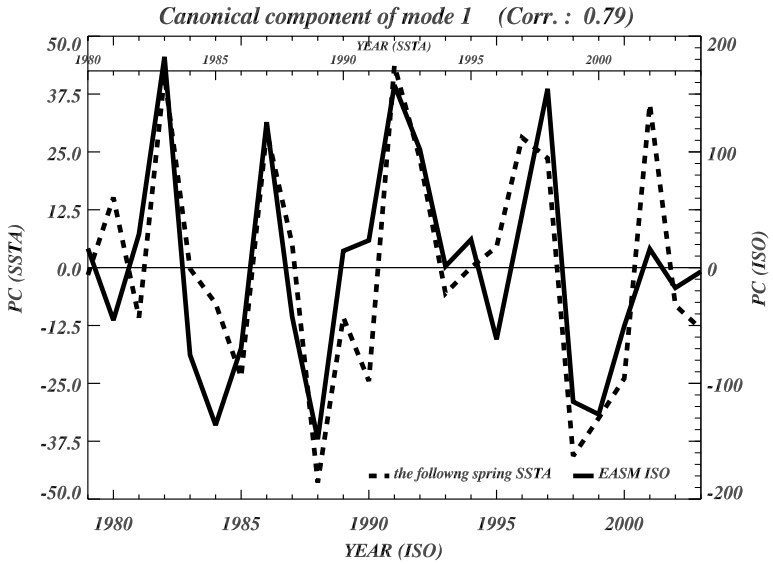

Fig. 11. Same as Fig. 10, except for the relationship between NISO in the EASM (predictor) and the following spring SSTA (predictand). The solid and dashed lines indicate the values for the NISO in the EASM and the following spring SSTA, respectively.

the predictand, the more the predicted pattern of eastern/central SST matches with the observed pattern. The canonical loading patterns for the SST and NISO are much similar to the first EOF structures shown in Fig. 9 (not shown).

In terms of the ENSO predictability, we also performed an analysis similar to Fig. 9, but used NISO as a predictor. The predictor (NISO) and predictand (the following spring SST anomalies) have the same domain as in the previous section, but the period for NISO is from 1979 to 2003 and that for SST is from 1980 to 2004. The first leading EOF pattern exhibits similar structures with those in Fig. 9 (not shown). However, the correlation between the associated time series exhibits a higher value of about −0.65. In particular, the two canonical component time series achieve a correlation coefficient of about 0.79 (Fig. 11). It is likely due to the outstanding and large variability of ENSO.

For the purpose of validation for CCA results, we took the parametric bootstrap procedure (e.g. Efron and Tibshirani, 1993). The observed and forecasted values are mostly determined by two canonical component time series. The bootstrap procedure is based on 10000 random samples of size 25. The resulting correlation coefficient between two canonical component time series is estimated from random samples. The 5th and 95th percentiles of the results are then used as 95% confidence level. For the NISO predictability, the lower and upper bounds are 0.07 and 0.83, respectively. Conversely, for the ENSO predictability, the lower and upper bounds are 0.59 and 0.91, respectively. The latter represents the true correlation coefficient

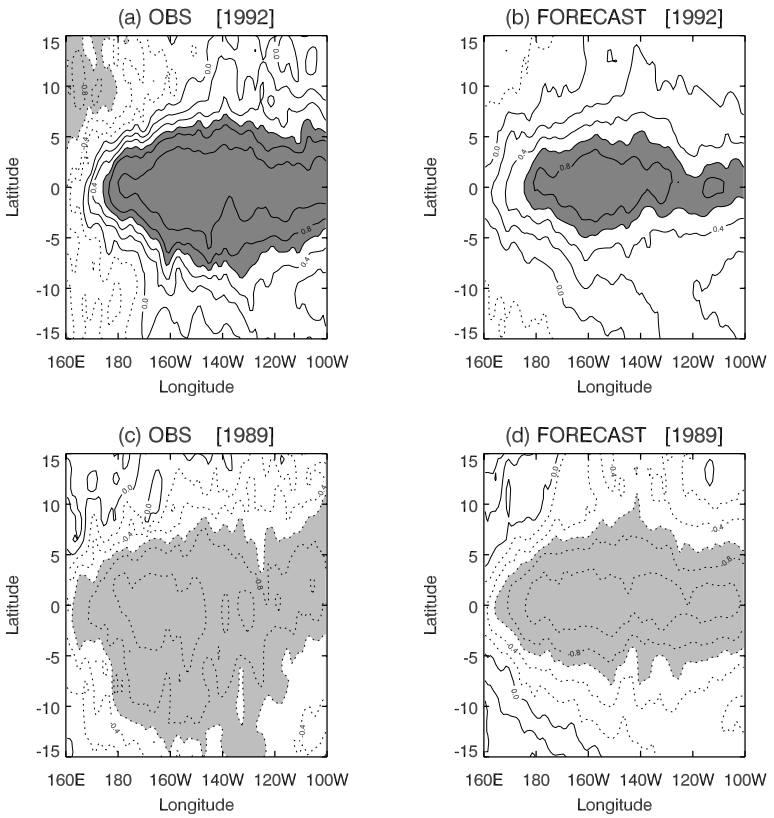

Fig. 12. The observed (a) [(c)] and predicted (b) [(d)] spring SST anomalies for the extreme case of 1992 (El Niño) [1989 (La Niña)].

better than the former. The former is characterized by considerable uncertainties. Of two cases, the ENSO predictability has a statically more significant and stable meaning than the NISO predictability. Actually, the forecasted pattern of the NISO has a more complex pattern due to various contributing factors and space-time structure of the NISO (not shown). Many studies support the limitation on the probability of monsoon or rainfall using ENSO (e.g. Lucero, 1998). In regards to the ENSO predictability, the patterns of the observed SST anomalies were also compared with patterns of the forecasted SST anomalies through CCA from 1980 to 2004 (not shown). We attempt to show only the extreme cases of El Niño (1992) and La Niña (1989) (Fig. 12). The ENSO structure predicted by NISO is reasonable. Note that it does not necessarily imply that NISO leads ENSO, although the ENSO predicted by NISO has a pattern well correlated with observations. We conclude that NISO can be used as an ENSO predictor. A diagnostic study using a statistical model, such as the CCA model, might lead to the improved predictability.

6. Discussion and conclusion

Of particular interest in the present work is the northward propagation of the 30–60-day EASM mode and its interannual variability in the EASM. In order to investigate a northward evolution of the ISO over East Asia, we conducted an EOF analysis of the filtered 30–60-day OLR data carried out with the temporal-latitudinal cross-section. We defined a northward propagation of the ISO as the first mode of the EOFs (i.e. 30–60-day EASM mode). The NISO corresponds to the northward propagating climatological ISO for the active/break monsoons. Its associated time series shows the interannual variability of the NISO. The ISO north of 25°N shows apparent out-of-phase changes with that south of 25°N. Even though the ISO has a significant standing component, the ISO in convection is dominated by the propagating component rather than the standing component (Zhang and Hendon, 1997).

The findings indicate that the principal NISO structure appears in its northward evolution of well-organized convection. The significance of the interannual variability of the NISO for ENSO in cases of lagged correlations, with QB characteristics through the preceding summer to the concurrent summer, was evident. We also performed the regression analysis of atmospheric and oceanic data. The NISO connects with the anomalous easterly wind and eastward evolution of the oceanic Kelvin wave. Consequently, QB-type ENSO, which is associated with the abrupt transition of ENSO, is closely tied with the NISO. There are enhanced anticyclonic anomalies in the WNP region during the concurrent summer. The anticyclonic anomalies are likely to play an important role in connecting the NISO with

QB-type ENSO, through the vertical wind shear mechanism. Although its complete role has not been determined yet, the NISO seems to be related to the development of the QB-type ENSO.

The impact of ENSO on the phase seems to be larger than the impact on the amplitude of the ISO. While most of the studies on EASM–ENSO relationship have focused on the intensity in the monsoon, Lim and Kim (2007) have demonstrated that ENSO causes a delay of the onset time in the EASM, through the Walker and Hadley circulation change associated with delayed Indian monsoon (e.g. westerly flow). In addition, Wu and Wang (2000) have reported that ENSO induces the delayed onset of the South China Sea WNP summer monsoon, and in turn the delayed onset time of the EASM. In this study, the phase dependency on ENSO is remarkably consistent with the delay of onset time in Wu and Wang (2000) and Lim and Kim (2007). Furthermore, Lu and Ren (2005) showed that the tropical 30–60-day ISO exhibits a phase difference according to the preceding ENSO phase (i.e. El Niño, La Niña and neutral) in the reasonable agreement with the present study. They have stated that the weakened easterly shear in the tropical region delays the phase of the northward propagating ISO. In the same manner, the strengthened easterly shear in the extratropical region may change the phase of the NISO in the EASM. It may be related to the reinforced WNP subtropical high. However, more investigation into the possible link between the meridional propagation and the QB-type ENSO is necessary.

Using the above findings, we also explored the predictability of the NISO and ENSO through the CCA method. The predictability on the ENSO has a statistically more significant meaning than that on the NISO. It suggests that the NISO would be a precursor to ENSO. The active and break phases of the NISO, which correspond to the climatological ISO cycle, seem to couple with the seasonal cycle related to the anomalous easterly wind and oceanic Kelvin wave, which in turn leads to the ENSO transition. The unpredictability of the NISO may be caused by a large year-to-year variability of the 30–60-day ISO due to many contributing factors, which should be investigated further. The problem of dynamical predictability of ENSO and NISO is a remaining issue and should be clarified throughout the modeling work in the future study. Such an attempt will improve the predictability of ENSO. Improving the understanding on the relationship with ENSO may shed a new light on the interaction between the tropics and the mid-latitudes. The causes and mechanisms associated with the QB-type ENSO on the time scale of the ISO should also be examined more extensively.

Acknowledgments

This work was funded by the Korea Meteorological Administration Research and Development Program under Grant CATER 2006-4205. This work was also supported by the second stage of the Brain Korea 21 Project.

References

Barnett, T. P. 1991. The interaction of multiple time scales in the tropical climate system. *J. Clim.* **4**, 269–285.

Chang, C. P., Zhang, Y. and Li, T. 2000. Interannual and interdecadal variations of the East Asian summer monsoon and tropical Pacific SSTs. Part I: Roles of the subtropical ridge. *J. Clim.* **13**, 4310–4325.

Chen, T. C. and Chen, J. M. 1995. An observational study of South China Sea monsoon during 1979 summer: Onset and life cycle. *Mon. Wea. Rev.* **123**, 2295–2318.

Efron, B. and Tibshirani, R. J. 1993. *An Introduction to the Bootstrap*. Chapman and Hall, London, 436 pp.

Ha, K.-J. and Lee, S.-S. 2007. On the interannual variability of the Bonin high associated with the East Asian summer monsoon rain. *Clim. Dyn.* **28**, 67–83.

Ha, K.-J., Park, S.-K. and Kim, K.-Y. 2005. On interannual characteristics of climate prediction center analysis precipitation over the Korean peninsula during the summer monsoon season. *Int. J. Climatol.* **25**, 99–116.

He, Y. and Barnston, A. G. 1996. Long-lead forecasts of seasonal precipitation in the tropical Pacifics islands using CCA. *J. Clim.* **9**, 2020–2035.

Hendon, H.-H., Zhang, C. and Glick, J. D. 1999. Interannual variation of the Madden-Julian oscillation during Austral summer. *J. Clim.* **12**, 2538–2550.

Hsu, H. H. and Weng, C. H. 2001. Northwestward propagation of the intraseasonal oscillation in the western North Pacific during the boreal summer: Structure and mechanism. *J. Clim.* **14**, 3834–3850.

Hwang, S. O., Schemm, J. K. E., Barnston, A. G. and Kwon, W.-T. 2001. Long-lead seasonal forecast skill in far Eastern Asia using canonical correlation analysis. *J. Clim.* **14**, 3005–3016.

Ji, M., Leetmaa, A. and Derber, J. 1995. An ocean analysis system for seasonal to interannual climate studies. *Mon. Wea. Rev.* **123**, 460–481.

Jiang, X. and Waliser, D. E. 2008. Northward propagation of the subseasonal variability over the eastern Pacific warm pool. *Geophys. Res. Lett.* **35**, L09814, doi:10.1029/2008GL033723.

Kalnay, E., Kanamitsu, M., Kistler, R., Collins, W., Deaven, D. et al. 1996. The NCEP/NCAR 40-year reanalysis project. *Bull. Amer. Meteor. Soc.* **77**, 437–471.

Kawamura, R., Murakami, T. and Wang, B. 1996. Tropical and midlatitude 45-day perturbations over the western Pacific during the northern summer. *J. Meteorol. Soc. Japan* **74**(6), 867–890.

Kim, K.-Y. 2002. Investigation of ENSO variability using cyclostationary EOFs of observational data. *Meteorol. Atmos. Phys.* **81**, 149–168.

Kim, K.-Y. and Kim, Y.-Y. 2002. Mechanism of Kelvin and Rossby waves during ENSO events. *Meteorol. Atmos. Phys.* **81**, 169–189.

Kug, J.-S. and Kang, I.-S. 2006. Interactive feedback between ENSO and the Indian Ocean. *J. Clim.* **19**, 1784–1801.

Lau, K. M. and Chan, P. H. 1986. Aspects of the 40–50 day oscillation during the northern summer as inferred from outgoing longwave radiation. *Mon. Wea. Rev.* **114**, 1354–1367.

Lau, K. M., Yang, G. J. and Shen, S. H. 1988. Seasonal and intraseasonal climatology of summer monsoon rainfall over East Asia. *Mon. Wea. Rev.* **116**, 18–37.

Lawrence, D. M. and Webster, P. J. 2001. Interannual variations of the intraseasonal oscillation in the South Asian summer monsoon region. *J. Clim.* **14**, 2910–2922.

Lim, Y.-K. and Kim, K.-Y. 2007. ENSO impact on the space-time evolution of the regional Asian summer monsoon. *J. Clim.* **20**, 2397–2415.

Li, Y., Lu, R. and Dong, B. 2007. ENSO-Asian monsoon interaction in a coupled ocean-atmosphere GCM. *J. Clim.* **20**, 5146–5177.

Lu, R. and Ren, B. 2005. The influence of ENSO on the seasonal convection evolution and the phase of 30–60-day oscillation during boreal summer. *J. Meteorol. Soc. Japan* **83**(6), 1025–1040.

Lucero, O. A. 1998. Effects of the southern oscillation on the probability for climatic categories of monthly rainfall, in a semi-arid region in the southern mid-latitudes. *Atmos. Res.* **49**, 337–348.

Madden, R. A. and Julian, P. R. 1971. Detection of a 40–50-day oscillation in the zonal wind in the tropical Pacific. *J. Atmos. Sci.* **28**, 702–708.

Meehl, G. A. 1997. The South Asian monsoon and the tropospheric biennial oscillation. *J. Clim.* **10**, 1921–1943.

Murakami, M. 1979. Large-scale aspects of deep convective activity over the GATE area. *Mon. Wea. Rev.* **107**, 994–1013.

Nitta, T. 1983. Observational study of heat sources over the eastern Tibetan Plateau during the summer monsoon. *J. Meteorol. Soc. Japan* **61**, 590–605.

Rasmusson, E. M., Wang, X. and Ropelewski, C. F. 1990. The biennial component of ENSO variability. *J. Mar. Syst.* **1**, 71–96.

Rayner, N. A., Parker, D. E., Horton, E. B., Folland, C. K., Alexander, L. V., et al. 2003. Global analyses of sea surface temperature, sea ice, and night marine air temperature since the late nineteenth century. *J. Geophys. Res.* **108**(D14), 4407, doi:10.1029/2002JD002670.

Shen, S. and Lau, K. M. 1995. Biennial oscillation associated with the East Asian summer monsoon and tropical sea surface temperatures. *J. Meteorol. Soc. Japan* **73**(1), 105–124.

Slingo, J. M., Rowell, D. P., Sperber, K. R. and Norney, F. 1999. On the predictability of the interannual behaviour of the Madden-Julian Oscillation and its relationship with El Niño. *Q. J. Roy. Meteorol. Soc.* **125**, 583–609.

Teng, H. and Wang, B. 2003. Interannual variations of the boreal summer intraseasonal oscillation in the Asian-Pacific region. *J. Clim.* **16**, 3572–3584.

Tsou, C. H., Hsu, P. C., Kar, W. S. and Hsu, H. H. 2005. Northward and northwestward propagation of 30–60 day oscillation in the tropical and extratropical western North Pacific. *J. Meteorol. Soc. Japan* **83**(5), 711–726.

Wang, B. and An, S.-I. 2005. A method for detecting season-dependent modes of climate variability: S-EOF analysis. *Geophys. Res. Lett.* **32**, L15710, doi:10.1029/2005GL022709.

Wang, B. and Rui, H. 1990. Synoptic climatology of transient tropical intraseasonal convection anomalies: 1975–1985. *Meteorol. Atmos. Phys.* **44**, 43–61.

Wang, B., Wu, R. and Li, T. 2003. Atmosphere–warm ocean interaction and its impacts on Asian–Australian monsoon variability. *J. Clim.* **16**, 1195–1211.

Wang, B. and Xie, X. 1996. Low-frequency equatorial waves in vertically sheared zonal flow. Part I: Stable waves. *J. Atmos. Sci.* **53**, 449–467.

Wang, B. and Xie, X. 1997. Northern hemisphere summer monsoon singularities and climatological intraseasonal oscillation. *J. Clim.* **10**, 1071–1085.

Wu, R. and Wang, B. 2000. Interannual variability of summer monsoon onset over the western North Pacific and the underlying processes. *J. Clim.* **17**, 277–289.

Wu, R. and Wang, B. 2001. Multi-stage onset of the summer monsoon over the western North Pacific. *Clim. Dyn.* **17**, 277–289.

Yasunari, T. 1990. Impact of Indian monsoon on the coupled atmosphere/ocean system in the tropical Pacific. *Meteorol. Atmos. Phys.* **44**, 29–41.

Yu, Z. P., Chu, P. S. and Schroeder, T. 1997. Predictive skills of seasonal to annual rainfall variations in the U.S. affiliated Pacific islands: Canonical correlation analysis and multivariate principal component regression approaches. *J. Clim.* **10**, 2586–2599.

Zhang, R. H., Sumi, A. and Kimoto, M. 1996. Impact of El Niño on the East Asian monsoon: A diagnostic study of the 86/87 and 91/92 events. *J. Meteorol. Soc. Japan* **74**, 49–62.

Zhang, C. and Hendon, H. H. 1997. Propagating and standing components of the intraseasonal oscillation in tropical convection. *J. Atmos. Sci.* **54**, 741–752.